Reflection Coefficient Calculation from Marine High Resolution Seismic Reflection (Chirp) Data and Application to an Archaeological Case Study

JONATHAN M. BULL[1], RORY QUINN[1,3], and JUSTIN K. DIX[2]

[1] *Department of Geology, Southampton Oceanography Centre, University of Southampton, Southampton SO14 3ZH, United Kingdom*
[2] *Department of Oceanography, Southampton Oceanography Centre, University of Southampton, Southampton SO14 3ZH, United Kingdom*
[3] *Now at Coastal Studies Research Group, School of Environmental Sciences, University of Coleraine, Coleraine BT52 1SA, United Kingdom*

(Received 15 August 1997; accepted 2 March 1998)

Key words: Chirp profilers, high resolution images, archaeological case study

Abstract. Chirp sub-bottom profilers produce high-resolution images of the near-surface. An attribute of the sea-bed reflection in chirp data are fluctuations in polarity between adjacent traces. Two models are proposed and presented to explain this: the first incorporates changes in an acoustic impedance gradient at the sea bed; the second uses changes in the thickness of the uppermost sediment layer. Mixing of adjacent traces produces a consistent polarity for the sea-bed reflector. Reflection coefficients are calculated, using amplitude information derived from single-traces, and polarity information from trace mixing, with application to a marine archaeological case study. The reflection coefficient calculated for the top of a buried 18th century wooden wreck is –0.26.

Introduction

Chirp profilers are marine high frequency (swept) sources with a pre-determined and repeatable source signature (Figure 1a). Chirp profilers typically operate in a range of 1–10 kHz, offer vertical resolution on a decimetre scale in the top c. 30 m of unconsolidated sediments, and are being increasingly used for marine environmental, archaeological and well-site surveys. A general discussion of chirp sources and optimal processing strategies is discussed in the accompanying paper (Quinn et al., accompanying paper in press); in the present paper the nature of the sea-bed reflector is examined together with its effect on the determination of reflection coefficients of deeper layers.

For high frequency sub-bottom profilers (2–8 kHz used here, corresponding to wavelengths of 75–19 cm) small lateral variations in the character of the seabed and very near-surface (top 30 cm) sediments have a profound effect on the sea-bed return. Reflections observed in seismic data are not always caused by discrete geologic horizons, but can be interference composites caused by many thinner interfaces (Mayer, 1979). Furthermore, the sea bed is frequently not a step change in acoustic impedance, but a gradational change with the sea-bed acoustic impedance gradient changing over small vertical as well as lateral distances. Boundary layer roughness, on spatial frequencies comparable to the acoustic source, also controls the sea-bed reflection.

As noted by Richardson and Briggs (1996) there are a number of factors that control the propagation and scattering of high frequency acoustic sound at or near the sea-bed including biological, geological, biogeochemical and hydrodynamic processes operating at the benthic boundary layer. Bioturbation of sediments by benthic animals affects the physical properties of marine sediments: burrowing, ingestion, defecation, tube building, biodeposition, cementation and metabolic activities modify porosity, density, grain size, compaction/cohesion, fabric and micro-topography (Richardson and Young, 1980). Richardson and Young (1980) suggest the overall effect (compared to unbioturbated sediments) is to lower compressional and shear wave velocities together with attenuation.

The amplitude of the sea-bed reflection is commonly used as a proxy for the far-field signature with which to compare the amplitudes of deeper reflections. This comparison is particularly important as it facilitates the calculation of reflection coefficients, which in turn place constraints on the nature of lithologies and objects present in the sub-surface. In this paper we show, and propose models to explain, that the apparent polarity of the sea-bed return on chirp profiles varies randomly from trace to trace. We show how polarity

Marine Geophysical Researches **20:** 1–11, 1998.

information can be obtained by considering adjacent traces, and illustrate how the amplitude and polarity of reflection coefficients can be determined from chirp data.

An archaeological site survey (of the Invincible, an 18th century wreck, East Solent, U.K.) is used as an example data set. Reflection coefficients derived from these data demonstrate how quantitative analysis of Chirp data can be used to predict the constituent material of buried artefacts. The advantage of using this data set is that previous work (Quinn et al., 1997) had predicted that wooden artefacts should give large and negative reflection coefficients.

Attributes of the Sea-Bed Reflector in Typical Chirp Data

Quinn et al. (accompanying paper in press) have established that the optimum display mode for Chirp data is after instantaneous amplitude conversion. This process, however, has a major disadvantage in that the data is down-shifted in terms of frequency content, and all polarity information is lost. The sea bed viewed on instantaneous amplitude sections is consistent in terms of amplitude and seismic attribute. However, when chirp data is viewed with the polarity information still present, the sea-bed reflector exhibits fluctuations in polarity between adjacent traces (see Figure 2a). Reflector polarity is determined by identifying the Klauder wavelet (Figure 1c) associated with the impedance response on each trace. Thus changes in the sign of the maximum of the cross-correlation function are interpreted as changes in polarity. Trace mixing can be used to determine a more consistent polarity for a reflector such as the sea bed (Figure 2b) and is discussed in more detail in the case study. For all the data discussed in this paper, the data acquisition was designed to ensure that the source ghost did not interfere with the sea-bed reflection: the source was towed close to the sea-surface in calm conditions so that the ghost could be identified in the upper part of the water column (for example, at c. 1 ms in Figure 5).

Modelling the Sea-Bed Reflector

As discussed earlier, bioturbation affects the physical properties of sediments and this, together with compaction and sediment mixing during deposition will produce vertical acoustic impedance profiles which prevent the sediment surface being considered as a step change in impedance.

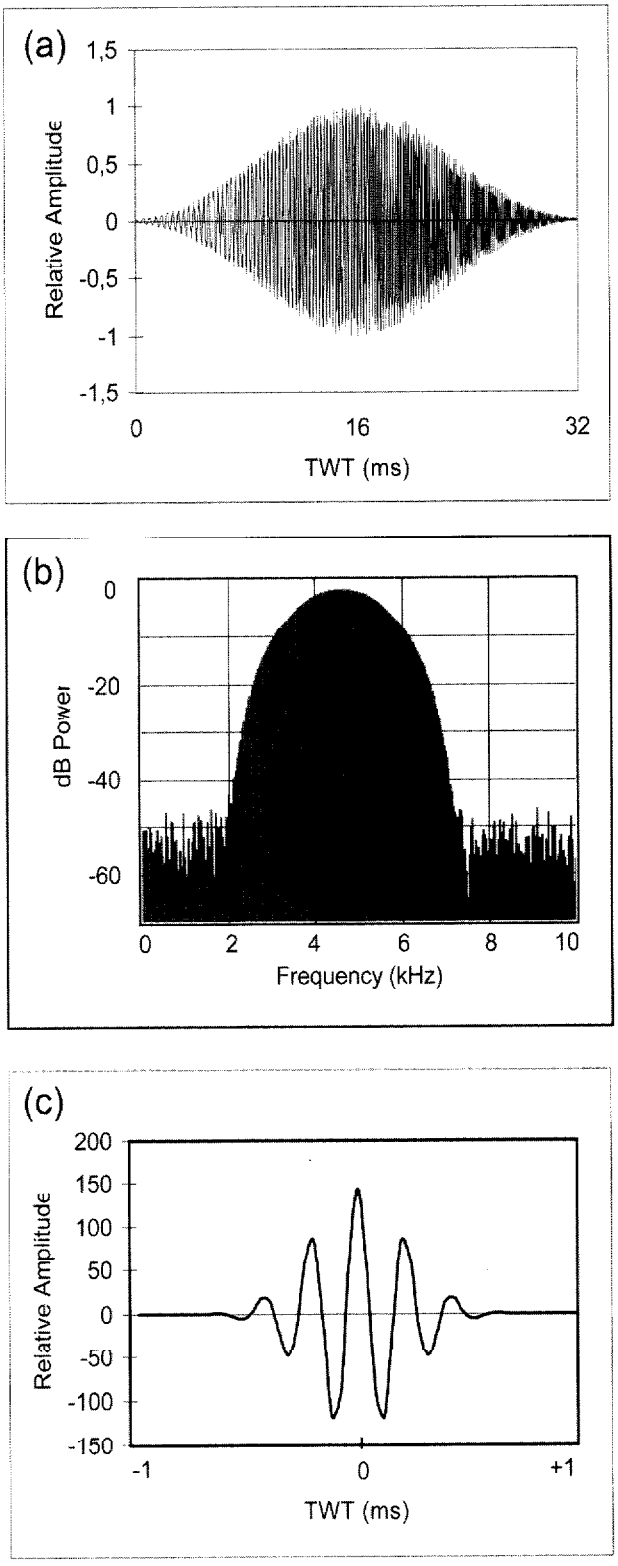

Fig. 1. (a) The 32 ms frequency modulated Chirp pulse, linearly sweeping from 2–8 kHz. (b) Power spectrum of the Chirp pulse. (c) Klauder wavelet – the autocorrelation of the Chirp pulse.

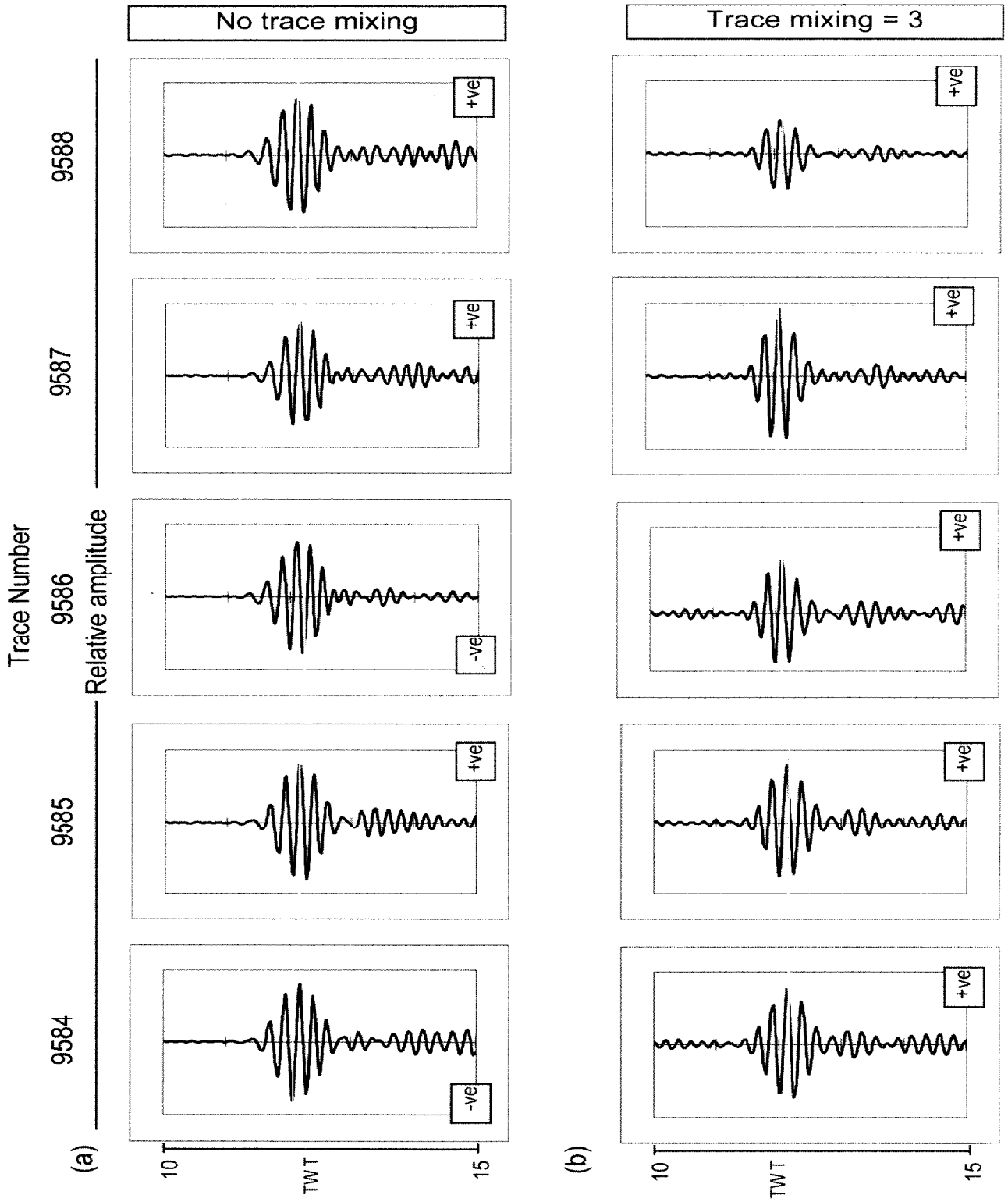

Fig. 2. Diagram of five adjacent correlated chirp traces from the Invincible site. (a) On individual traces note the apparently random polarity changes of the reflected disturbances from the sea bed at approximately 12 ms. The polarity of the sea-bed reflection is determined by the position of the maximum amplitude, indicated by the grey vertical line. (b) After application of a trace mixing (using a 3 trace running mix). There is 0.6 m spacing between each trace.

In order to examine the effect of geo-acoustic layering of the sea bed on the chirp pulse, the authors modelled two cases: a *transition zone* model and a *variable surficial sediment thickness* model. The first model follows Schock (1996) in treating the sea bed as a stratified fluid and investigates how an acoustic impedance gradient (a transitional sea bed) and associated interference effects from composite reflections affects the polarity of the frequency modulated chirp pulse. The second model determines how varying surficial sediment thickness changes the polarity of the chirp pulse.

Schock (1996) synthesised the acoustic impedance variation found in marine near-surface well-logs and concluded that interlayer transitions were typically in the range of 0.05–0.3 m thickness. In the models that follow we investigate the top 0.3 m of sediments below the sea-bed, and use a range of impedances ($1.5–3 \times 10^6$ kg m^{-2} s^{-1}) that are commonly found in near-surface sediments (Schock, 1996). The interlayer 'thickness' used in the models is 40 μs ($\sim$0.03 cm) which corresponds to the sampling interval of the chirp data. This sampling interval is very much less than the dominant acoustic wavelength (19–75 cm) of the source and ensures that the models have sufficient resolution. The models were convolved with the auto-correlated chirp pulse – the Klauder wavelet (Figure 1c) and the synthetic traces generated were then examined. The modelling procedure was to increment in 40 μs steps (which corresponds to increments of 0.032 m, assuming a compressional wave velocity of 1600 m s^{-1}); the results presented in Figures 3 and 4 are representative of the full range of models completed.

Figure 3 summarises the results for a transition zone at the sea bed. The thickness of the transition zone ranges from 40 μs (model 1, approximately 0.032 m) to 400 μs (model 4, approximately 0.32 m). Model 1 represents a step change in acoustic impedance between the water column and the sea bed, and the synthetic trace generated is the same shape as the auto-correlation of the chirp sweep (Klauder wavelet) as expected. As the thickness of the transition zone increases, and hence the acoustic impedance gradient decreases, the polarity and shape of the sea bed return changes. For example, in model 3 the polarity of the sea bed is reversed (from positive to negative). Within the full range of models completed there were random changes in the sea-bed polarity.

The second case illustrating the role of the thickness of the surficial layer is shown in Figure 4, where the separation distance between the two reflectors varies from 80μs to 168 μs (c. 0.06 m to 0.13 m). Figure 4 shows a selection of the models that were run, and demonstrates that when the reflectors are closely spaced the apparent polarity can change sign for very small changes in bed thickness (a 0.032 m change between models 2 and 3).

It can be concluded that either one, or a combination, of the two models presented can produce polarity reversals for small changes in the sea-bed geometry. The magnitude of these changes is sufficiently small that they are likely to occur on a spatial scale of centimetres to metres, and produce the apparent polarity reversals seen between adjacent traces. The trace separation distance of 0.6 m is less than the fresnel zone radius of 0.9–1.8 m, for the 2–8 kHz source and a water depth of 9 m, and hence there is overlap in information on immediately adjacent traces.

Calculation of Reflection Coefficients

Reflection amplitudes are altered by many stages in seismic processing and hence when attempting to calculate absolute reflection coefficients it is most valid to work with single-fold unprocessed data. In this paper the original uncorrelated data has been correlated with the source sweep, but no further processing has been undertaken. For interpretation purposes chirp data is amenable to a series of processing procedures as described by Quinn et al. (accompanying paper in press), but not considered further here.

The following analysis assumes normal incidence and is valid for angles of incidence of less than 15° (Sheriff and Geldart, 1995). For the acquisition system used, the offset between source and receiver was 3.5 m, and means that reflection coefficients should be considered valid for water depths of greater than 6.5 m. In the case study discussed below the water depth was greater than 9 m, which equates to a maximum angle of incidence of 11°. The analysis also assumes that the air/water interface has a reflection coefficient of –1. For the high frequency source we are using it is worthwhile considering the validity of this: as the wavelength of the acoustic system approaches the wavelength of the waves on the sea surface the value of this coefficient changes. Chapman and Scott (1964) derived an empirical relationship between the scattering strength (or reflection loss), the incidence angle (defined as the angle between the acoustic ray and the horizontal) and wind speed for acoustic sources which ranged between 100 and 6400 Hz. Their results indicated that, for the frequency range investigated, the scattering was source-frequency independent. Using their relationships, for an incidence angle of 80°, and a typical wind speed of 5 m·s^{-1}, the reflection loss was 0.72 dB.

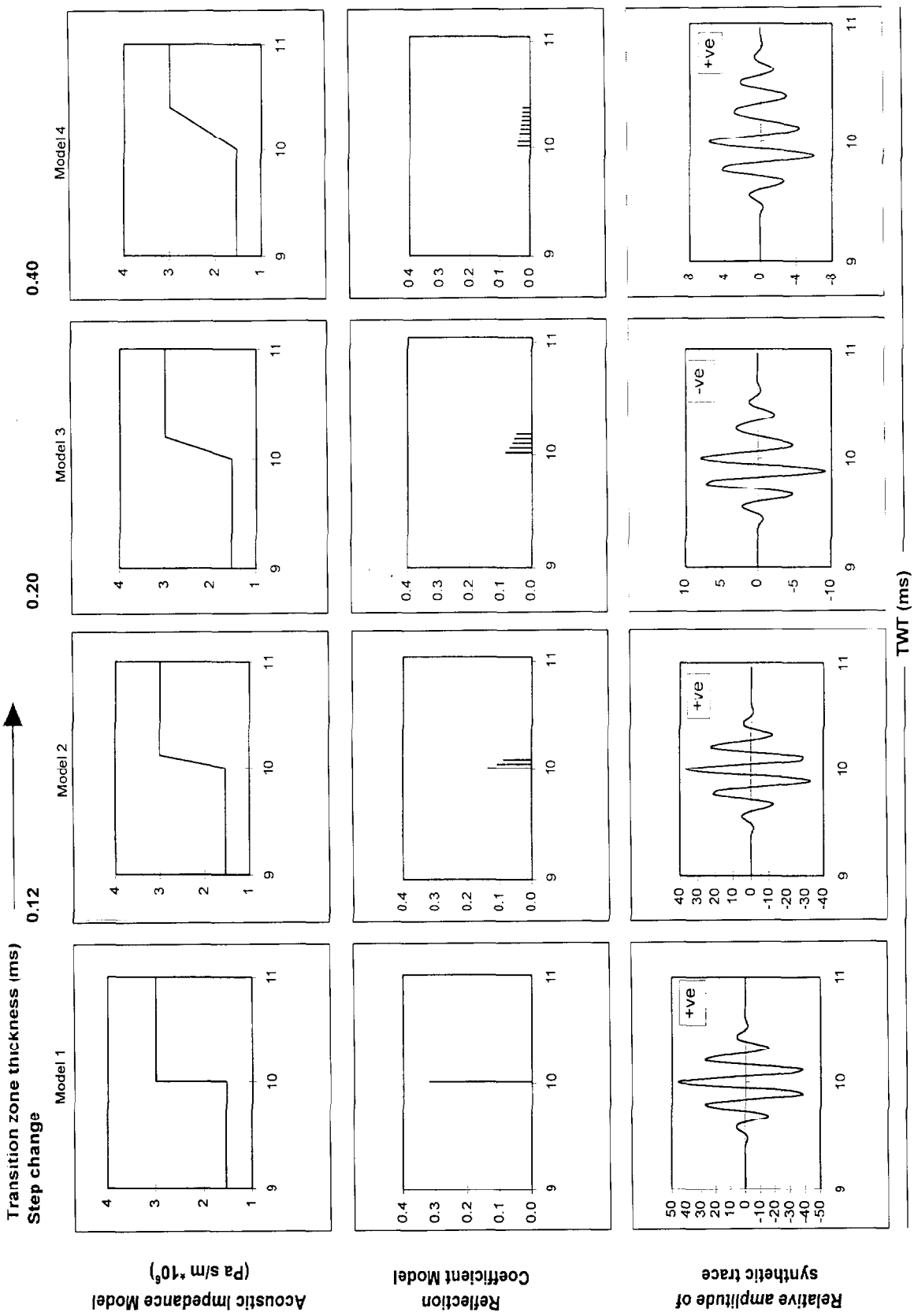

Fig. 3. Diagram illustrating the effects of an acoustic impedance gradient at the sea bed on the polarity of the auto-correlated Chirp pulse. Model 1 represents a step change in acoustic impedance between the water column and the sea bed. Models 2 through 4 model the sea bed as a stratified fluid, where the sea bed is sub-divided into layers of thickness 40 μs (corresponding to the sampling interval of the Chirp pulse). Note that the polarity of the pulse is reversed in model 3 (from positive to negative)

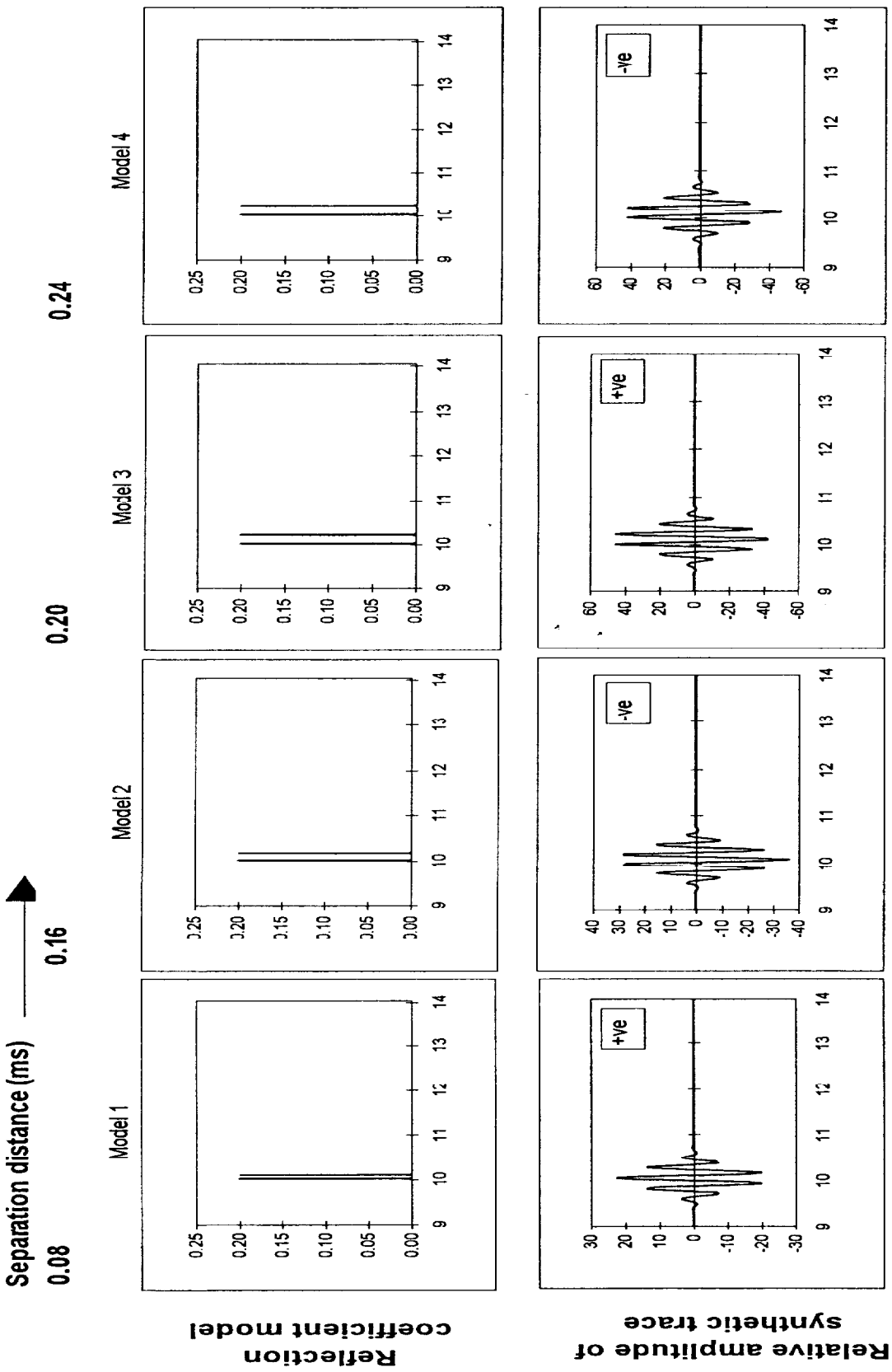

Fig. 4. Diagram illustrating the effect of changes in the thickness of the surface sediment layer on the polarity of the auto-correlated Chirp pulse. Note the change in the polarity of the pulse between models 2 and 3 for a layer thickness change of only 0.032 m.

TABLE I

Summary of polarity and reflection coefficient information for the Invincible site

Reflector	Magnitude of reflection coefficient $\|K_R\|$	Standard deviation (s)	Reflector polarity (no trace mixing)	Reflector polarity (trace mixing = 3)	Reflection coefficient K_R
Sea floor (primary)	|0.43|	0.18	54% positive 46% negative	79% positive 21% negative	+0.43
Deeper reflector (wreck)	|0.26|	0.12	36% positive 64% negative	31% positive 69% negative	−0.26

Kuperman (1990) considered the specular reflection and transmission of an acoustic plane wave at a randomly rough sea surface. The sea surface was described by the Pierson-Moskowitz model spectrum for a fully developed sea. Kuperman (op. cit.) derived reflection coefficients as functions of source frequency, incidence angle, wind speed and direction of wind. In the case study discussed later the sea state was calm with a wind speed of less than 5 m s^{-1}, and, from the two studies above, the loss in reflection strength from the sea surface is c. 0.7–0.8 dB. Thus reflection coefficients calculated below may be under-estimated by 8–10%.

The effects of scattering by rough surfaces is considered to be sufficiently small to be ignored for the short travel paths considered here, and are not incorporated within the expressions for the reflection coefficients. Frequency dependent absorption is also not explicitly considered in the general analysis below, but is discussed later for the case study.

Following Anstey (1977), Warner (1990) and Spence et al. (1995) reflection coefficients of the sea floor $K_{R(SF)}$ and a deeper reflection $K_{R(DR)}$ can be calculated from chirp data using the following relationships:

$$K_{R(SF)} = \frac{TWT_m}{TWT_p}\frac{A_m}{A_p} \quad (1)$$

$$K_{R(DR)} = K_{R(SF)}\frac{TWT_{DR}}{TWT_p}\frac{A_{DR}}{A_p} \quad (2)$$

where A_p, A_m and A_{DR} are the amplitudes of the primary sea-floor reflector, the first multiple of the sea-floor reflector and the deeper reflector, respectively, and TWT_p, TWT_m and TWT_{DR} are the corresponding two-way times. These expressions incorporate a correction for spherical spreading, which is proportional to the two-way time. Amplitudes for the sea-bed reflection, the multiple and the deeper reflection of interest can be picked directly from single-channel correlated sections.

Calculation of the polarity of reflection coefficients is dependent on determination of the polarity of individual reflectors. From the previous section it is clear that, due to the very high frequency nature of the chirp source, small changes in the composition or geometry of the uppermost 0.3 m of the sea bed can change the apparent polarity of the sea-bed reflection. This makes routine determination, using single traces, of the polarity of reflection coefficients of deeper reflections difficult, except where the sea bed represents a step change in acoustic impedance, and the deeper event is particularly strong and discrete. Trace mixing (Figure 2b) – a running average over adjacent traces with equal weight, was used to combine adjacent traces to determine the polarity of reflections. The trace mixing averages out the bioturbation and small-scale lateral changes in the stratigraphy to leave a simpler interface from which the polarity can be determined. In summary, reflection coefficients are calculated using amplitude information from single traces and polarity information from trace mixing. In the next section a marine archaeological case study is used to show how reflection coefficients of strong sub-surface events are calculated from chirp data.

Case Study – The Invincible, An 18th Century Shipwreck

Quinn et al. (1997) show that wooden material buried within unconsolidated sediments will give a strong negative sub-surface reflector. The Invincible site (East Solent, U.K.) was chosen as a site for testing the methodology, outlined above, for calculating reflection coefficients. This site offered the opportunity to acquire data over an 18th century oak wreck partially buried by well-sorted, fine-grained (2.25–2.47 phi) quartzoze sands. The geophysical survey was conducted using a 100 kHz side-scan sonar together with a 2–8 kHz swept frequency chirp system in an average water depth of 10 m with a transmit rate of four pulses per second. Navigation data, with an

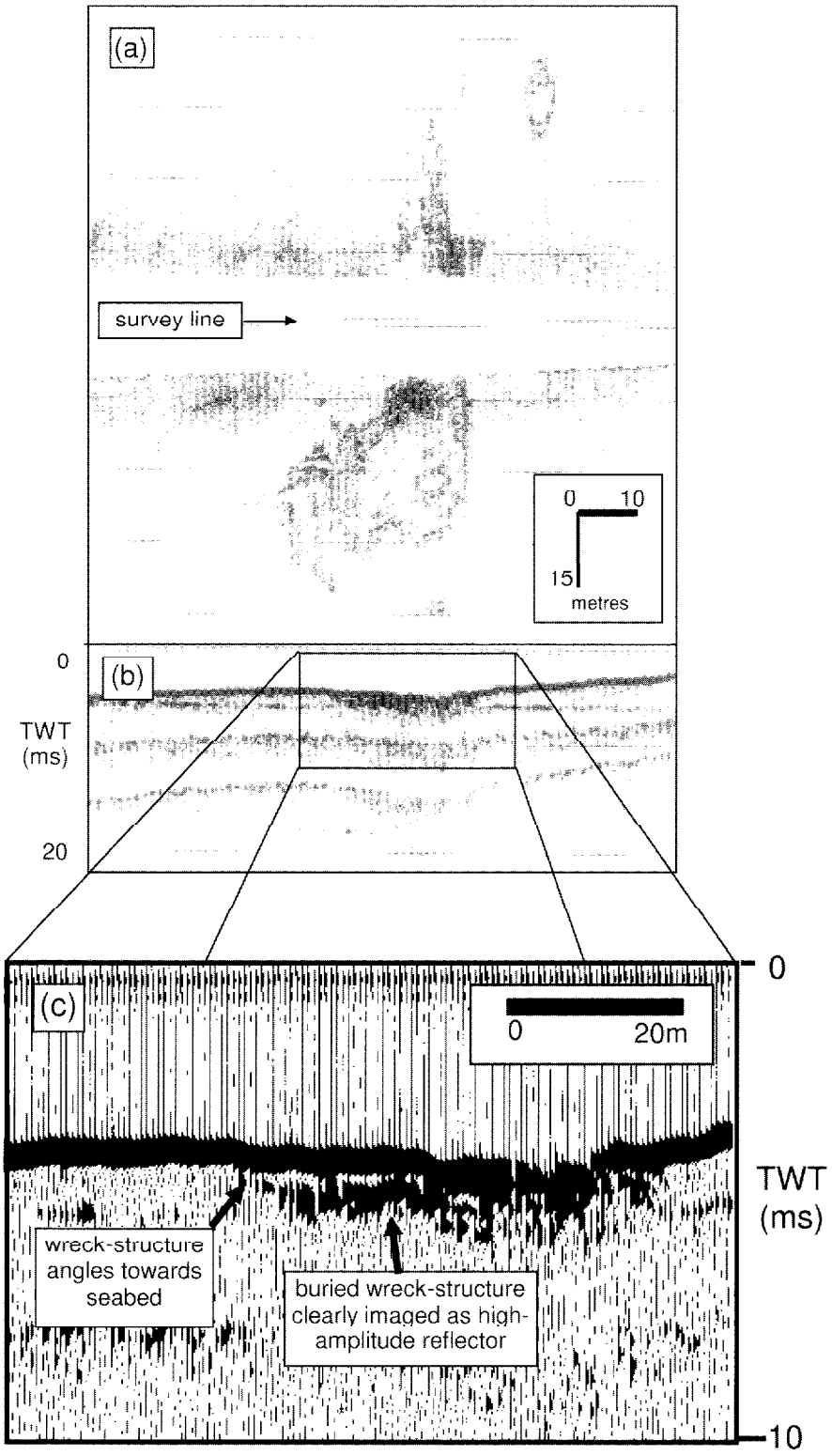

Fig. 5. Composite image of the Invincible site, East Solent, U.K. (a) A dual channel 100 kHz sonograph of the wreck acquired using a GeoAcoustics dual frequency side-scan sonar. (b) The corresponding instantaneous amplitude correlated chirp profile acquired using a GeoAcoustics Chirp system. (c) An enlarged bandpass filtered section of (b).

accuracy of ±1 m, was provided by a differential global positioning system.

Figure 5 is a composite image of one line acquired over the site incorporating sidescan (a) and chirp data (b, c) displayed after the instantaneous amplitude conversion described by Quinn et al. (in press). These data were acquired over the centre of the semi-buried wreck, surveying from the buried starboard-side of the Invincible to the partially exposed port-side (left to right in the above diagram). The side-scan sonar image shows that a substantial portion of the wreck was exposed on the sea bed at the time of the survey. The band-pass filtered profile of section (c) images the buried portside of the wooden wreck as a high amplitude reflector, providing proof that reflection seismology can image buried wooden artefacts.

Table I summarises the results of the calculation of the reflection coefficient of the sea bed and the buried wood using equations (1) and (2): The sea bed has a reflection coefficient of +0.43, while the buried wood has a reflection coefficient of –0.26. The polarity of the two reflection coefficients was deduced (or confirmed in the case of the buried wood) by trace mixing. A series of tests were designed to find the smallest number of traces needed in the running mix to ensure a consistent sea-bed polarity, while minimising the loss in spatial resolution. For the Invincible site, a 3-trace running mix was chosen on the basis of the results of the tests. For the shallow burial of wood (<0.1 ms) use of standard Q-correction techniques to correct for frequency dependent absorption (see for example Sheriff and Geldart, 1995), suggest that, the reflection coefficient of wood may be underestimated by 30%. This together with errors caused by considering the sea surface as a reflector with coefficient –1, discussed earlier, means that for a worst case, the wood reflection coefficient may be under-estimated by 40%.

One method for testing the validity of the reflection coefficient calculation is to do forward modelling. Figure 6a shows a single trace over the buried wreck and, with comparison to adjacent traces (Figure 5c), it is clear that there are two events — the sea bed and the buried wreck. Figure 6b shows a model for the trace with reflection coefficients of 0.43 for the sea bed and –0.26 for the wreck with a separation of 0.6 m. The synthetic generated by convolving the model with the Klauder wavelet is shown in Figure 6c. Note the closeness of the fit between the real data (grey) and the synthetic (black), indicating the validity of the approach. A separation distance between the sea bed and the buried wreck of other than 0.6 m (±0.1 m) resulted in a poorer fit between the synthetic and the observed data. This uniqueness means that the depth

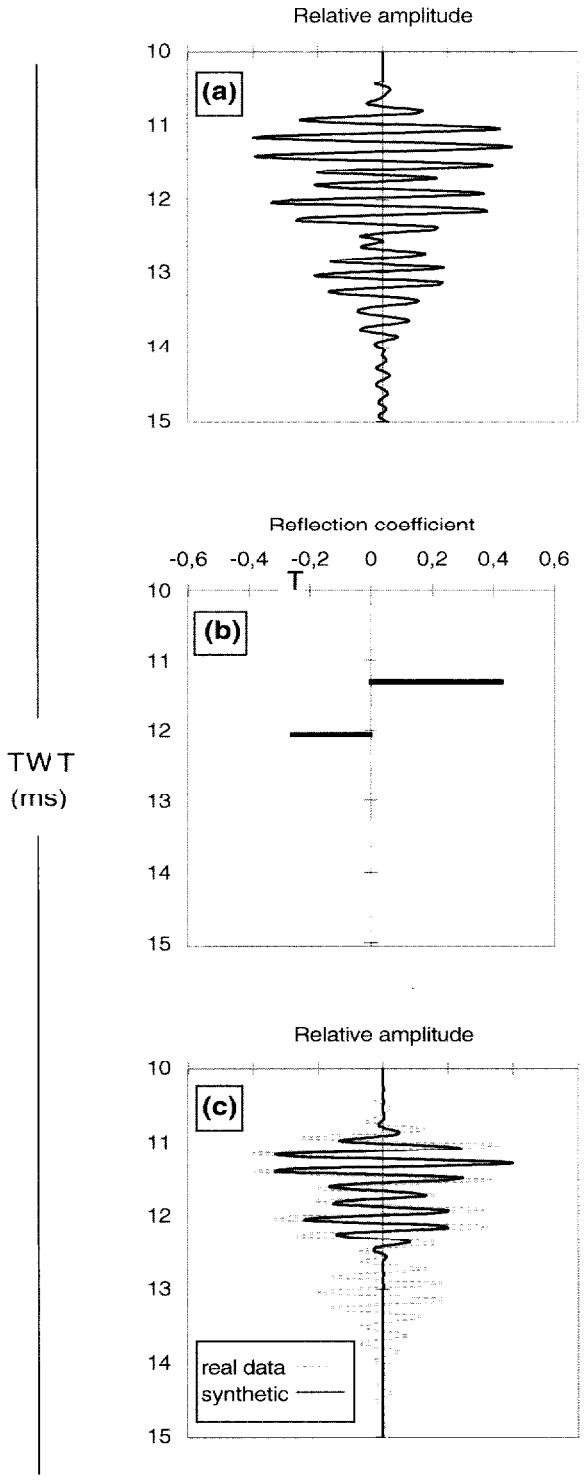

Fig. 6. (a) Single trace over the a buried portion of *The Invincible*. (b) Model incorporating reflection coefficients calculated for the sea bed and the wreck reflector. (c) Synthetic trace (black) produced by convolving the Klauder wavelet with the model. Note the excellent fit between the observed data (grey) and the synthetic.

TABLE II

Table of wood density, Young's modulus (E), Poisson's ratio (μ), and the compressional wave velocities calculated for eleven wood species assuming that the wood planks act as elastic plates, where at least one sample dimension is smaller than the dominant wavelength of the incident compressional wave. L, R and T refer to the three wood axes defined in Figure 7

Wood species	Density kgm^{-3}	E_L GNm^{-2}	E_R GNm^{-2}	E_T GNm^{-2}	μ_L	μ_R	μ_T	V_L ms^{-1}	V_R ms^{-1}	V_T ms^{-1}
Ash	670	15.8	1.51	0.80	0.49	0.38	0.20	5570	1620	1120
Beech	750	13.7	2.24	1.14	0.48	0.41	0.20	4870	1890	1260
Birch	620	16.3	1.11	0.62	0.46	0.41	0.20	5780	1470	1020
Maple	590	10.0	1.52	0.87	0.48	0.46	0.22	4690	1810	1250
Mahogany	530	12.4	0.97	0.48	0.43	0.43	0.22	5360	1500	980
Oak	660	5.3	2.14	0.97	0.42	0.39	0.19	3120	1960	1230
Walnut	590	11.2	1.19	0.63	0.56	0.39	0.20	5260	1540	1050
Poplar	380	9.7	0.89	0.41	0.36	0.36	0.17	5420	1640	1050
Douglas Fir	480	15.7	1.06	0.78	0.37	0.21	0.19	6160	1520	1300
Scots Pine	580	16.3	1.10	0.57	0.47	0.36	0.16	6010	1480	1000
Spruce	390	10.7	0.71	0.43	0.45	0.27	0.17	5870	1400	1070

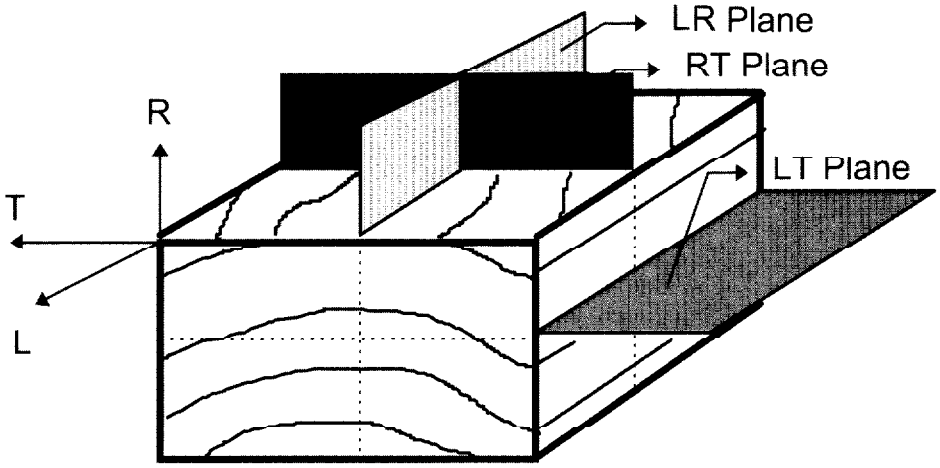

Fig. 7. Diagram for illustrating the three planes of elastic symmetry in wood: LR – Longitudinal-Radial plane, RT – Radial-Tangential plane and LT = Longitudinal-Tangential (after Quinn et al., 1997).

of burial of the top of the wreck can be predicted with confidence.

The value of a large and negative reflection coefficient for wood buried in unconsolidated sediments is in agreement with Quinn et al. (1997) who used experiments and theoretical models to conclude that reflection coefficients calculated for oak buried in the marine sediments range between –0.03 and –0.64. This large range of values is mainly due to the highly anisotropic nature of wood (see Table II), whilst the magnitude of the reflection coefficient is dependent upon the orientation of the incident compressional wave relative to the axes/planes of elastic symmetry (Figure 7). Table II summarises the results of Quinn et al. (1997) for eleven wood species and shows that compressional wave velocities parallel to the wood grain (V_L) are consistently faster than those across grain (V_R and V_T).

Discussion and Conclusions

This paper has shown that Chirp sub-bottom profilers are capable of producing high resolution images of the sub-surface. The central frequency of the chirp

bandwidth (2–8 kHz) is 4.6 kHz which equates to a theoretical resolution (Rayleigh criterion) of 0.09 m in the very near-surface, for the fine sandy sediments (velocity 1600 m s^{-1}) in the area of the case study. Practical resolution however is lower due to the rapid attenuation of the higher frequencies.

Small changes in the nature of the sea bed can affect the nature of the sea-bed return in Chirp data and in particular change its apparent polarity. Two cases have been modelled and shown to be possible explanations. The first involved an acoustic impedance gradient at the sea bed, while the second investigated the effect of interference between the top and bottom interfaces of the layer at the sea bed. Schock (1996) concluded that an interlayer transition between two homogeneous sediment units acts as a low-pass filter. It is clear, however, that such a transition zone not only affects the frequency component of the reflection data, but interference effects also cause apparently random changes in reflected events. Similar phenomenon is seen in the models of varying surficial sediment thickness.

Reflector polarity information can be ascertained from Chirp data by combining adjacent traces which has the effect of averaging out bioturbation and small-scale lateral changes in stratigraphy. Reflection coefficients can be estimated by using average amplitude information from individual traces and polarity information from trace mixing.

An archaeological case study illustrated the capabilities of chirp data for high resolution near-surface studies. The reflection coefficient of buried wood (Oak buried in unconsolidated marine sands) of –0.26 agrees with the theoretical and experimental studies of Quinn et al. (1997).

Acknowledgements

The authors thank GeoAcoustics Ltd, Great Yarmouth, U.K. for permission to publish the chirp pulse, Dr R.B. Whitmarsh for useful discussion, and to two anonymous reviewers whose comments helped to improve the final manuscript. This research was funded by NERC grant GR3/9533.

References

Anstey, N. A., 1977, Seismic Interpretation: The Physical Aspects, Boston (Int. Human Rights Dev. Corp.).

Chapman, R. D. and Scott, H. D., 1964, Surface Backscattering Measured Over an Extended Range of Frequencies and Grazing Angles, *J. Acoust. Soc. Am.* **36**, 1735–1737.

Kuperman, W. A., 1990, Coherent Component of Specular Reflection and Transmission at a Randomly Rough Two-Fluid Interface, *J. Acoust. Soc. Am.* **58**, 365–370.

Mayer, L., 1979, The Origin of Fine Scale Acoustic Stratigraphy in Deep-Sea Carbonates, *J. Geophys. Res.* **84**, 6177–6184.

Quinn, R., Bull, J. M., and Dix, J. K., 1997, Imaging Wooden Artefacts Using Chirp Sources, *Archaeological Prospection* **4**, 25–35.

Quinn, R., Bull, J. M., and Dix, J. K., 1998, Optimal Processing of Marine High-Resolution Seismic Reflection (Chirp) Data, *Mar. Geophys. Res.* **20**, 13-20.

Richardson, M. D. and Briggs, K. B., 1996, In Situ and Laboratory Geoacoustic Measurements in Soft Mud and Hard-Packed Sand Sediments: Implications for High-Frequency Acoustic Propagation and Scattering, *Geo-Marine Letters* **16**, 196–203.

Richardson, M. D. and Young, D. K., 1980, Geoacoustic Models and Bioturbation, *Mar. Geol.* **38**, 205–218.

Schock, S. G., 1996, Predicting Vertical Profiles of Sediment Properties from Seismograms, *Oceanology Intl Conference Proceedings* **1**, 1–20.

Sheriff, R. E. and Geldart, L. P., 1995, *Exploration Seismology*, Cambridge University Press.

Spence, G. D., Minshull, T. A., and Fink, C., 1995, Seismic Studies of Methane Gas Hydrate, Offshore Vancouver Island. In Carson, B., Westbrook, G. K., Musgrave, R. J., and Suess, E. (Eds.) *Proc. ODP, Sci Results* **146** (Pt 1), College Station, Tx (Ocean Drilling Program) 163–174.

Warner, M., 1990, Absolute Reflection Coefficients from Deep Seismic Reflections, *Tectonophysics* **173**, 15–23.